Compact chip-scale filter based on curved waveguide Bragg gratings

Steve Zamek,* Dawn T. H. Tan, Mercedeh Khajavikhan, Maurice Ayache, Maziar P. Nezhad, and Yeshaiahu Fainman

Department of Electrical and Computer Engineering, University of California, San Diego, 9500 Gilman Drive, La Jolla, California 92093-0407, USA
**Corresponding author: szamek@ucsd.edu*

Received July 22, 2010; accepted August 29, 2010;
posted September 17, 2010 (Doc. ID 132114); published October 13, 2010

We propose a method for miniaturization of filters based on curved waveguide Bragg gratings, so that long structures can be packed into a small area on a chip. This eliminates the stitching errors introduced in the fabrication process, which compromise the performance of long Bragg gratings. Our approach relies on cascading curved waveguide Bragg gratings with the same radius of curvature. An analytical model for the analysis of these devices was developed, and a filter based on this model was designed and fabricated in a silicon on insulator platform. The filter had a total length of 920 μm, occupied an area of 190 μm × 114μm , and exhibited a stop band of 1.7 nm at 1.55 μm and an extinction ratio larger than 23 dB.

OCIS codes: 130.2790, 130.7408.

Waveguide Bragg gratings find numerous applications ranging from semiconductor lasers to on-chip interconnects [1,2]. More recent works have demonstrated the capability of wavelength tuning and dispersion engineering [3–7], to name a few. After more than two decades of intensive research, chip-scale Bragg gratings remain appealing because of their high reflectivity and comparatively easy fabrication process. The bandwidth and the extinction ratio of the transmission spectrum are easily tailored by choosing an appropriate periodic perturbation strength, grating length, and apodization profile. Numerous applications require narrow bandwidth, achieved by long Bragg gratings with weak periodic perturbation, whose lengths exceed the typical lithographic write field. Whether the fabrication is done using electron-beam (e-beam) lithography or photolithography, the lithographic field is limited in size. Therefore, the performance of long Bragg gratings is compromised by the errors in the stitching of multiple fields [8,9]. The capability of "packing" the long Bragg gratings into a given area is of utmost importance for miniaturization of filters, reflectors, photonic crystals, and other nanophotonic components.

In this Letter we propose the miniaturization of waveguide Bragg gratings into curved waveguide Bragg gratings, as shown in Fig. 1(a). An arbitrary Bragg grating with a total length L can be packed into the desired area A using a cascade of curved waveguide Bragg gratings. Using the same radius of curvature R for all sections eliminates the need to adjust the period of the Bragg grating for each section separately, as the dispersion relation is identical for all sections. It is easy to verify that the layout shown in Fig. 1(a) attains packing efficiency, defined as the dimensionless parameter $L/\sqrt{A}$, of approximately $\sqrt{\pi L/4R}$. Although more efficient packing schemes exist, it is obvious that a smaller radius of curvature is desirable. However, how small can the radius of curvature R be without having an impact on the optical properties of the grating?

To address this question, it is instrumental to consider a simpler structure, consisting of a periodic array of curved waveguide Bragg gratings, depicted in Fig. 1(b). Each section has a shape of an arc with radius R, and the junctions between the sections are shown by broken red lines. These junctions are step discontinuities, where some scattering occurs because of the mode mismatch in two consecutive sections. The two sources of loss are therefore the scattering at the junctions and radiation losses owing to bending. As the radius of curvature gets smaller, both losses increase. We will next investigate the effect of decreasing the radius of curvature on the optical properties of the Bragg grating.

The transmission coefficient through the cascade of N identical curved Bragg gratings can be found using the transmission matrix approach. Following this approach, the field at any point along the structure is given by the superposition of two counterpropagating modes with amplitudes A and B. For a section of our structure, shown in Fig. 1(c), the modal amplitudes at the input,

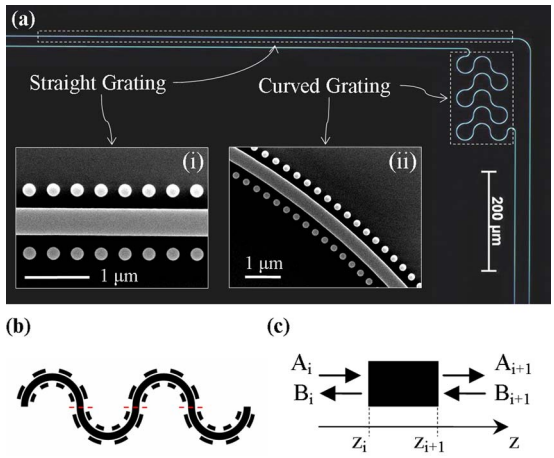

Fig. 1. (Color online) (a) Dark-field micrograph of the fabricated structures: the marking shows the curved and the straight gratings of the same length. Insets (i) and (ii) show SEM micrographs of the straight and the curved gratings, respectively. (b) Array of curved waveguide Bragg gratings. (c) Schematic of the transmission matrix formalism.

A_i and B_i, can be related to those at the output, A_{i+1} and B_{i+1}, via the transmission matrix [10]:

$$\begin{bmatrix} A_{i+1} \\ B_{i+1} \end{bmatrix} = T \begin{bmatrix} A_i \\ B_i \end{bmatrix} = \begin{bmatrix} (1-\alpha)t'^{-1} & -r't'^{-1} \\ -rt^{-1} & t^{-1} \end{bmatrix} \begin{bmatrix} A_i \\ B_i \end{bmatrix}, \quad (1)$$

where $r = B_i/A_i$ and $t = A_{i+1}/A_i$ (with $B_{i+1} = 0$) are the reflection and transmission coefficients, α is the power-loss coefficient, and the prime sign designates the complex conjugate. From energy conservation, it follows that $|r|^2 + |t|^2 + \alpha = 1$, and the determinant of the matrix equals unity. Equation (1) shows the general form of the transmission matrix of a reciprocal element. We will now find the transmission matrices for the two elements comprising our structure—curved Bragg gratings and the junctions between them.

For a section of curved-waveguide Bragg grating of length L_b, the coefficients r and t in Eq. (1) can be found from the coupled-mode theory [2]: $r_b = -\kappa'[j\Delta\beta + S\coth(SL_b)]$ and $t_b = S[j\Delta\beta \sinh(SL_b) + S\cosh(SL_b)]^{-1}$, where $S = \sqrt{|\kappa|^2 - \Delta\beta^2}$, $\Delta\beta = \beta - \pi/\Lambda$, Λ is the Bragg grating period, κ is the coupling coefficient, and β is the complex propagation constant of the mode. The transmission matrix of a curved Bragg grating is given by

$$T_b = \begin{bmatrix} (1-\alpha_b)t_b'^{-1} & -r_b' t_b'^{-1} \\ -r_b t_b^{-1} & t_b^{-1} \end{bmatrix}, \quad (2)$$

where the subscript b stands for the Bragg grating. For zero losses (β is real and $\alpha_b = 0$), the result is in full agreement with previous work [11].

The reflection and transmission coefficients, r_j and t_j, associated with the junctions, are found numerically. For a small mode mismatch, the transmission coefficient is real and the reflection can be neglected [12]. The transmission matrix of a junction simplifies to

$$T_j \approx \frac{1}{t_j} \begin{bmatrix} (1-\alpha_j) & 0 \\ 0 & 1 \end{bmatrix}, \quad (3)$$

where the subscript j stands for junction, and the power conservation requires $t_j^2 + \alpha_j = 1$. Therefore, the transmission matrix for a junction is fully determined by the loss α_j, which is obtained numerically as discussed below.

Transmission through a cascade of N curved Bragg gratings with discontinuities between them is described by the total transmission matrix $T_0 = (T_b T_j)^N$. The matrix T_0 is obtained explicitly by diagonalization of the matrix $T_b T_j$, and the transmission coefficient through the cascade is calculated from the $(2,2)$ element of matrix T_0:

$$t_0 = (T_0)_{2,2}^{-1} = \frac{(\eta - \eta^{-1})}{(\eta^N - \eta^{-N})t_b^{-1}t_j^{-1} - (\eta^{N-1} - \eta^{1-N})}, \quad (4)$$

where $\eta = x/2 + \sqrt{(x/2)^2 - 1}$ and $x = (1-\alpha_j)(1-\alpha_b)t_b'^{-1}t_j^{-1} + t_b^{-1}t_j^{-1}$. The validity of Eq. (4) can be readily verified for some particular cases. For instance, for a single element ($N = 1$), Eq. (4) simplifies to $t_0 \approx t_b t_j$ as anticipated. For an infinite cascade of lossy elements ($\alpha_j + \alpha_b > 0$ and $N \to \infty$), it is easy to show that $t_0 \to 0$. For a cascade of waveguides with no losses ($\alpha_b = \alpha_j = 0$ and $t_b = t_j = 1$), $\eta = 1$, and $t_0 = 1$.

The expression in Eq. (4) simplifies to a transmission coefficient of a straight Bragg grating with no losses when the following condition is met:

$$(\alpha_b + \alpha_j)N \ll 1. \quad (5)$$

This is better understood by noticing that the left-hand side of condition 5 describes the amount of total loss in the entire structure. In other words, the condition assures no degradation of the insertion loss.

For demonstration of the proposed structure, we designed straight and curved waveguide Bragg gratings in a silicon on insulator (SOI) platform, with the dimensions shown in Fig. 2(a). The advantage of SOI is a high index contrast, and therefore strong modal confinement and low bending loss. The relation between the distance of the bumps from the guide, G, and the coupling coefficient, κ, was found from three-dimensional FEM simulations and is shown in Fig. 2(b). To obtain a filter with a target stop band of 1.6 nm, we chose the coupling coefficient $\kappa = 80$ cm^{-1} and filter length 920 μm [13]. As Fig. 2(b) suggests, this coupling is achieved for distance $G \approx 100$ nm between the guide to the bumps.

To analyze the losses (parameters α_b and α_j), we simulated a resonator based on two curved waveguides with a junction, depicted in Fig. 2(c). Perfect electric conductors were used as its mirrors so that the Q factor is defined solely by the internal losses, α_b and α_j. For a given curvature R, we simulated a resonator based on two

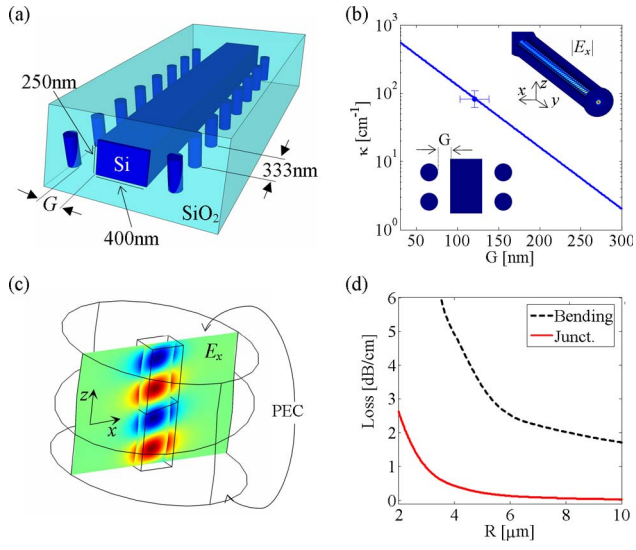

Fig. 2. (Color online) Design of the filter. (a) Schematics of the waveguide Bragg grating. (b) Coupling coefficient (log scale) as a function of the gap between the cylinders and the waveguide, obtained from 3D FEM simulations, as shown in the upper inset. The point marked by the blue dot corresponds to the fabricated structure with $G = 115 \pm 15$ nm and $\kappa = 80 \pm 15$ cm^{-1}. (c) A resonator used to analyze the losses, based on two curved waveguides with a junction in the joint. (d) Normalized losses obtained from the Q factor of the resonator, as a function of the curvature radius of the waveguide: bending loss, $\alpha_b/\pi R$ (dashed black curve) and loss at a junction, $\alpha_j/\pi R$ (solid red curve).

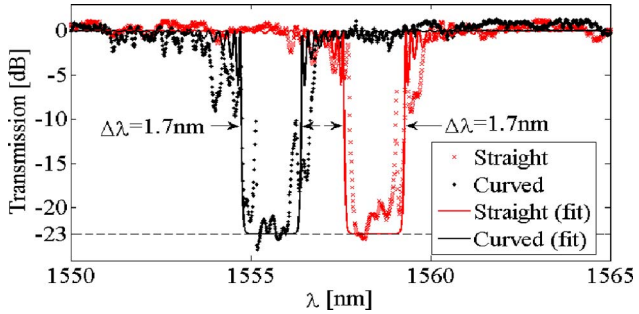

Fig. 3. (Color online) Measured transmission spectra for straight (red crosses) and curved (black dots) gratings. The solid curves show the fitted transmission spectra of Bragg gratings with $\kappa = 90\ \mathrm{cm}^{-1}$, $n_g = 4.27$, $L = 920\ \mu\mathrm{m}$, and $n_e = 2.340$ for the straight grating and $n_e = 2.336$ for the curved grating, with a constant background 23 dB below the signal.

curved waveguides joined together and compared the results to a resonator based on a single bent waveguide. By comparing the Q factors of the two resonators, it is possible to separate between the bending losses and the losses due to the scattering at the junction. The results are shown in Fig. 2(d), where, to express the loss per unit length, we normalized the parameters α_b and α_j by the factor πR. The radius of curvature was chosen to be $R = 19\ \mu\mathrm{m}$, for which the total loss is below 2 dB/cm, the fraction of power, $\alpha_b + \alpha_j$, lost at a segment with a circumference of $L_b = \pi R \approx 60\ \mu\mathrm{m}$ is below 0.003, and, for a total of $N = 15$ segments, condition (5) is satisfied. Therefore, according to the developed analytical model, the structure should exhibit a response identical to that of a straight grating of the same length.

Straight and curved waveguide Bragg gratings with a total length of 920 μm were fabricated on an SOI wafer, with Si thickness of 250 nm, on top of a layer of thermal oxide with a thickness of 3 μm, using e-beam lithography with a write-field size of $500\ \mu\mathrm{m} \times 500\ \mu\mathrm{m}$. Both structures had the same perturbation period $\Lambda = 333$ nm and the same waveguide cross sections, as shown in Fig. 2(a). The input and output waveguides were gradually tapered to the width of 110 ± 10 nm. The sample was then diced and cleaved across the tapered sections of the waveguide.

Transmission spectra were obtained by coupling a tunable laser source into the tapered waveguides on the sample through a tapered polarization-maintaining (PM) fiber. The output waveguide of the device, also tapered, was imaged through a free-space polarizer onto a detector connected to a power meter. The measured transmission spectra for the straight and curved Bragg gratings are shown in Fig. 3 by red crosses and black dots, respectively. The measured extinction ratio of both structures is higher than 23 dB, which is the limit, imposed by the PM tapered fiber. Both gratings exhibit a stop band width of 1.7 nm, which corresponds to $\kappa = 90\ \mathrm{cm}^{-1}$. These parameters are slightly larger than those we used in the design (1.6 nm and $\kappa = 80\ \mathrm{cm}^{-1}$), owing to the deviation of waveguide widths from the designed values. The two devices exhibit similar spectral response, with a shift of ~2.6 nm, attributed to the dispersion of the bent waveguide. Since the dispersion of a bent waveguide is known, this shift can be precompensated in the design stage to produce the stop band at the desired wavelength. Aside from the offset, the curved Bragg grating has a spectral response similar to that of a straight grating, as predicted by the developed model.

To summarize, we demonstrated straight and curved filters based on waveguide Bragg gratings. Both filters had a total length of 920 μm, a stop band of 1.7 nm, and an extinction ratio larger than 23 dB. The curved structure occupied an area of $190\ \mu\mathrm{m} \times 114\ \mu\mathrm{m}$, attaining packing efficiency of $L/\sqrt{A} \approx 6.2$. Nevertheless, it exhibited the same performance as its straight counterpart. The proposed approach opens a route to avoid the stitching errors present in the typical lithographic process of long structures. The developed analytical model aims to assist in the design of such structures in the future.

The authors wish to thank the Nano3 staff at UCSD and Bill Mitchell at UCSB for their support with the fabrication, Kazuhiro Ikeda from Nara Institute of Science and Technology for fruitful discussions, and Sun Labs at Oracle for their guidance and kind remarks. Financial support from the Defense Advanced Research Projects Agency (DARPA), the National Science Foundation (NSF), the NSF Engineering Research Center for Integrated Access Networks, the United States Air Force Office of Scientific Research (USAFOSR), and the United States Army Research Office (USARO) is greatly appreciated.

References

1. L. A. Coldren and S. W. Corzine, *Diode Lasers and Photonic Integrated Circuits* (Wiley, 1995), Chap. 3, pp. 65–111.
2. A. Yariv, *Optical Electronics*, 3rd ed. (Holt McDougal, 1985), Chap. 13, pp. 402–421.
3. H.-C. Kim, K. Ikeda, and Y. Fainman, J. Lightwave Technol. **25**, 1147 (2007).
4. H. C. Kim, K. Ikeda, and Y. Fainman, Opt. Lett. **32**, 539 (2007).
5. D. T. H. Tan, K. Ikeda, R. E. Saperstein, B. Slutsky, and Y. Fainman, Opt. Lett. **33**, 3013 (2008).
6. D. T. H. Tan, K. Ikeda, and Y. Fainman, Opt. Lett. **34**, 1357 (2009).
7. D. T. H. Tan, K. Ikeda, and Y. Fainman, Appl. Phys. Lett. **95**, 141109 (2009).
8. V. V. Wong, J. Ferrera, J. N. Damask, T. E. Murphy, H. I. Smith, and H. A. Haus, J. Vac. Sci. Technol. B **13**, 2859 (1995).
9. I. Petermann and S. Helmfrid, Appl. Opt. **44**, 4375 (2005).
10. R. F. Harrington, *Time-Harmonic Electromagnetic Fields* (McGraw-Hill, 1961), Chap. 8, p. 381–400.
11. M. Yamada and K. Sakuda, Appl. Opt. **26**, 3474 (1987).
12. D. Marcuse, *Light Transmission Optics* (Van Nostrand Reinhold, 1972), Chap. 9, pp. 379–386.
13. D. C. Flanders, H. Kogelnik, R. V. Schmidt, and C. V. Shank, Appl. Phys. Lett. **24**, 194 (1974).